Open Access Online Journal on Astronomy and Astrophysics

Acta Astrophysica Taurica

www.astrophysicatauricum.org

Acta Astrophys. Tau. 6(1), 1–4 (2025)

Analysis of events during the M 2.5 flare on June 7, 2011

Yu.A. Kupryakov[1,2], V.A. Maliutin[1], K.V. Bychkov[1], O.M. Belova[1], A.B. Gorshkov[1]

[1] Sternberg Astronomical Institute, Moscow State University, Universitetsky pr. 13, Moscow 119234, Russia
[2] Astronomical Institute of the Czech Academy of Sciences, Fričova 298, 25165 Ondřejov, Czech Republic
e-mail: kupry@asu.cas.cz

Received 10 August 2024

ABSTRACT

The object under study is the fragments of the falling matter during the M 2.5 flare in the NOAA AR 11226 on June 7, 2011. Observations were carried out with the horizontal solar installation HSFA-2 and the multichannel flare spectrograph MFS (Ondřejov Observatory). The traces of fragments were found in the CaII H, Hα, and Hβ lines. After reducing the line spectra, absorption fluxes were calculated for four moments of time, and a system of equations was solved for the populations of discrete levels and the ionization state of the hydrogen atom and CaII ion. The source of radiation was considered in the approximation of a homogeneous layer of heated gas. The gas parameters were selected in such a way that the observed and theoretical fluxes coincide with an accuracy of better than 5%. Calculations have shown that the temperature range T varies from 7 to 12 thousand K, the column concentration N is 1–5 10^{19} cm^{-2}, and the turbulent speed varies from 6 to 21 km/s.

Key words: chromospheric flare, prominence, radiation flux, homogeneous layer of heated gas

1 Introduction

Flare processes in the lower solar atmosphere are usually observed in the form of two parallel ribbons with radiation in a wide range of the electromagnetic spectrum. Emission from such ribbons can be stimulated by the precipitation of accelerated particles, Joule heating due to electric currents, a thermal flux of electrons from the primary energy release site, or by a combination of these processes acting together. The standard flare model (Brown, 1971) assumes that the primary energy release occurs due to magnetic reconnection. The process takes place high in the corona. Phenomena in the lower layers of the atmosphere represent a reaction to this energy release. However, there is evidence that energy release can occur directly in the lower regions of the solar atmosphere (Fletcher et al., 2011). In this case, flare ribbons can also be generated by the initial energy release in the lower layers of the solar atmosphere. The flare arcade is of great importance for understanding solar flares, since the scattering rate of possible heat sources strongly depends on the value of the so-called filling factor of the emitting plasma. The fine structure of the flare, noted back in Severnyi (1957), is also of great importance. Recently, Krucker et al. (2011) discussed the results of optical observations of flare ribbons with HINODE for the "thick target" model. The fluxes of nonthermal electrons per unit area, estimated within the framework of this model, can only be explained by the assumption of an unexpectedly high density of accelerated electrons. In this situation, smaller values of the filling factor can lead to even more extreme values of the flux density of nonthermal particles. In addition, X-ray, microwave, and radio emission clearly originates from many organized thin loops (Zimovets et al., 2013), which are also observed by TRACE in the UV range (Xu et al., 2012). Thus, observations of flare kernels in the visible and near-infrared ranges should be investigated and discussed.

2 Observations

The SOL2011-06-07 flare was observed by us with two spectrographs MFS and HSFA-2 (Ondřejov Observatory). The flare onset occurs at 6:16 UT, the impulsive phase lasts from 6:16 UT to about 6:45 UT, and the decay phase lasts more than two hours. Figure 1 shows an image assembly: the spectrum in the Hα line, the slit-jaw (SJ) image of the chromosphere and the prominence position, the spectrum and the chromosphere image at 06:40:34 UT, and the prominence image at 08:00:35 UT. All images were obtained with the MFS spectrograph.

Table 1. Flux values for four moments of time measured in erg/s/cm^2. Calculation error: Hα, CaII H – < 5 %, Hβ – < 10 %. The decimal order of the number is indicated in parentheses.

Time	07:52:46	08:01:46	08:02:03	08:05:11
Hα	1.73(+6)	1.18(+6)	2.68(+6)	3.03(+6)
Hβ	5.50(+5)	1.60(+5)	5.90(+5)	5.90(+5)
CaII H	6.52(+5)	3.02(+5)	6.14(+5)	8.07(+5)

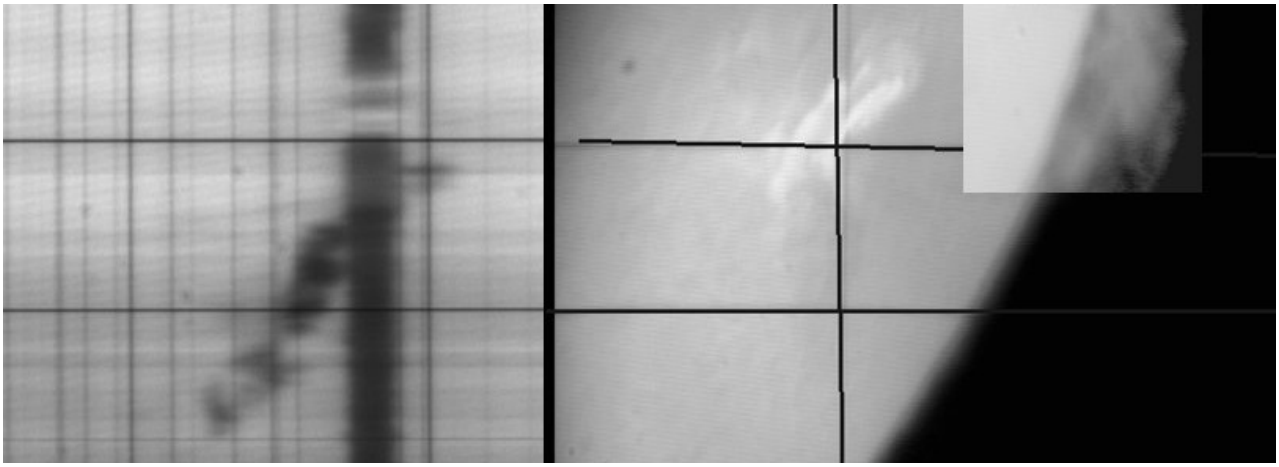

Fig. 1. Assembly of MFS frames (from left to right): Hα spectrum, SJ, prominence.

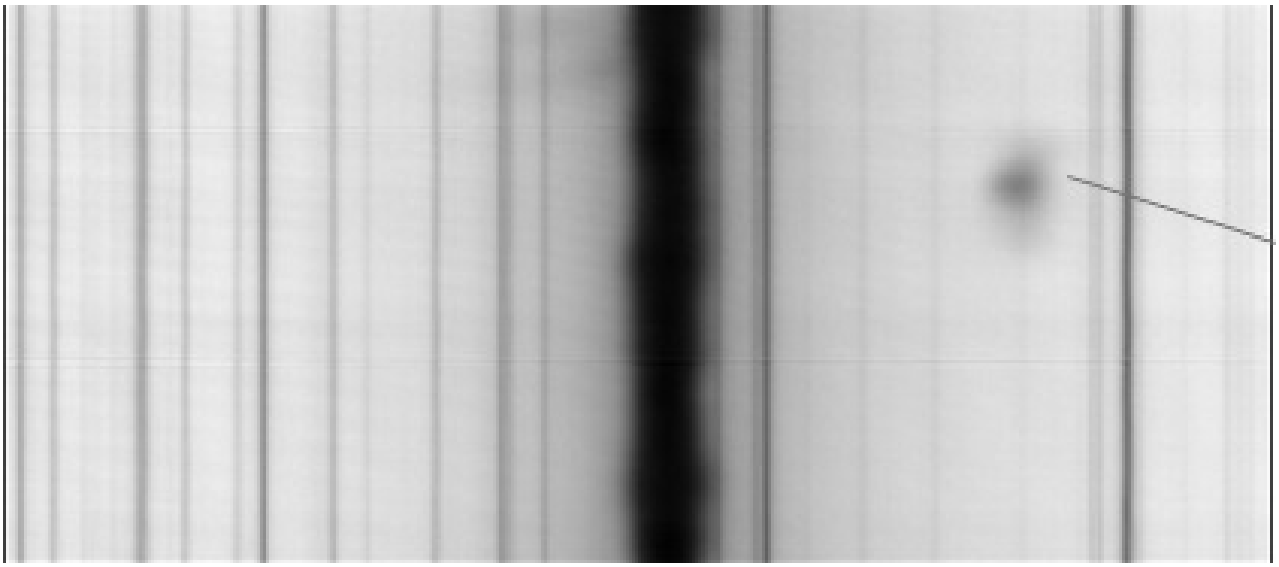

Fig. 2. Spectrum in the Hα line and a trace of the prominence fragment (the position is marked by a segment). The radial velocity value is 270 km/s.

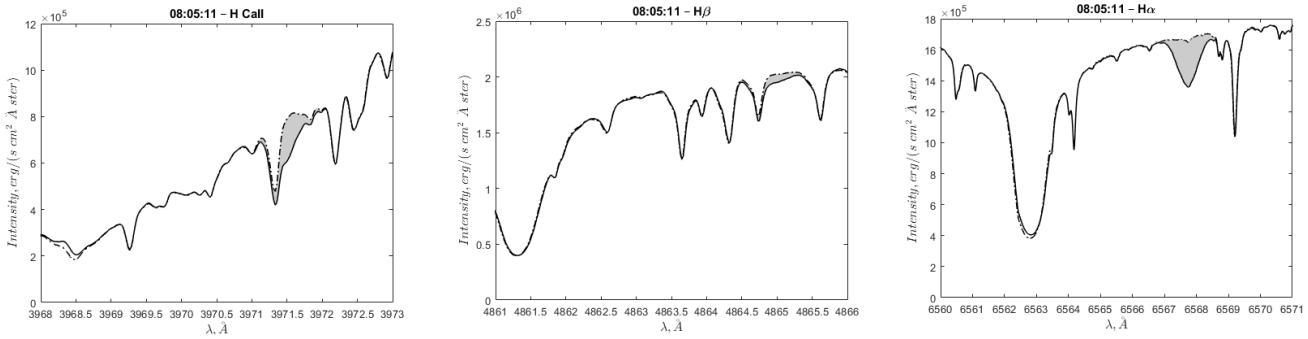

Fig. 3. Profiles of the CaII H, Hβ, and Hα lines (the shaded areas correspond to fluxes in erg/s/cm^2).

Figure 2 shows the spectrum in the Hα line obtained with the HSFA-2 spectrograph (a falling prominence fragment is clearly visible). This spectrograph allows for simultaneous observations in the CaII H, Hϵ, Hβ, D3, Hα, and CaIR 8542 Å lines. Four moments with a clearly visible prominence fragment on the SJ image were selected for processing. After taking into account flat-field and dark frames, line profiles were constructed considering the emission of

the chromospheric background (see Fig. 3). It can be seen that the traces of these fragments were detected only in the CaII H, Hβ, and Hα lines. Then the flux values were determined in erg/s/cm^2 (Table 1).

3 Calculation method

A system of equations for the populations of discrete levels and the ionization state of the hydrogen atom and CaII ion was solved. The main elementary processes of the level population were taken into account: bound-bound, bound-free, and free-bound collisional and radiative transitions in the field of photospheric radiation (considered to be blackbody with a temperature of $T_{\rm ph}$ = 5500 K). The hydrogen atom model includes 18 discrete levels, and the calcium ion model includes 22 levels. The scattering in spectral lines is taken into account in the approximation of the quantum escape probability. The atomic data of the HI atom are taken from Johnson (1972). The atomic data of the CaII ion are taken from the following sources: NIST (energy of levels and oscillator strengths in absorption), TOPBASE, Cunto, Mendoza (1992) (photoionization cross sections), Melendez et al. (2007) (collisional excitation and deactivation), Seaton (1964) (collisional ionization). The absorption coefficient profile of hydrogen lines was determined by the convolution of the Doppler and Holtsmark contours, and in calcium lines by the Voigt profile. The radiation was considered in the approximation of a homogeneous layer of heated gas. The gas parameters were selected in such a way that the observed and theoretical fluxes coincide with an accuracy better than 5 %. The parameters include the gas concentration n (cm^{-3}), the layer thickness L (km), the column density N (cm^{-2}) (which is the product of the previous two), the temperature T (K), the turbulent velocity $v_{\rm turb}$ (km/s), as well as $T_{\rm Ca}$ (K) is a parameter that imitates the contribution of the Lyman series (older than Lyβ) to the photoionization rate of calcium, which in terms of meaning is the temperature of a black body.

4 Calculation results

Table 2 shows the ranges of parameters of the gas layer: τ_α is the optical thickness in the Hα line, $\tau_{\rm H}$is the optical thickness in the CaII H line, and F(H), F(8542) are the fluxes in the CaII H line and the calcium infrared line.

Table 2. Calculated parameters of the emitting gas for each observation moment.

Parameter	7:52:46	8:01:46	8:02:03	8:05:11
N (10^{19} cm^{-2})	3.0–5.0	0.9–1.2	2.2–4.5	2.0–4.4
T (10^3 K)	6–8	6–18	8–11	10–12
$v_{\rm turb}$ (km/s)	6–7	9–10	15–18	20–21
$T_{\rm Ca}$ (10^3 K)	6.4–6.6	6.35–6.6	6.85–7.0	6.8–6.9
τ_α	1.4–1.5	0.2–0.3	~0.9	~0.7
$\tau_{\rm H}$	1.0–2.4	0.1–0.16	0.1–0.14	~0.1
F(H)/F(8542)	2.0–4.0	9.0–10.6	11.2–11.5	11.0–11.3

When explaining the emission in the studied lines, Joule dissipation is considered to be the source of heating and luminescence of the gas. From Table 2 it can be seen that even when analyzing the emission in three optical lines, it is possible to significantly limit the range of parameters of the gas layer. Within a specific time moment, the range of variation of the column density is about two times, and for the rest of the input parameters (T, $v_{\rm turb}$, $T_{\rm Ca}$), it is much smaller. An exception is the time moment 08:01:46 UT at which weak fluxes (F(Hβ), F(H CaII) ~ 10^5 erg/s/cm^2) and a large ratio of F(Hα)/F(Hβ) allow a wide range of parameters. The wide range of realizable values of the column density is caused by the transparency of the considered lines; thus, except for the first observation moment 7:52:46 UT, the optical thickness in the three registered lines is less than unity (see columns τ_α and $\tau_{\rm H}$ in Table 2). The transparency of the gas is also reported by the ratio of fluxes in the Balmer lines F(Hα)/F(Hβ). The growth of this ratio over time is explained by the increasing transparency in the Hα line, which in turn is caused by an increase in the microturbulent velocity $v_{\rm turb}$. A reliable limiter of possible values of the input parameters is the absence of registered emission in the HeI D3 line and the CaII IR λ = 8542 Å line. Thus, the upper limit of the values of the column density and temperature in Table 2 was fixed precisely based on the theoretical values of the flux in the D3 line, which in the calculations were limited to ~10^5 erg/cm^2/s. It is the order of magnitude that the weakest observed fluxes have. Table 3 provides specific examples of the input parameters of the gas layer and other calculated quantities.

Table 3. Examples of the calculated fluxes and gas parameters; fluxes are given in units of erg/s/cm^2. The decimal order of the number is indicated in parentheses.

Parameter	7:52:46	8:01:46	8:02:03	8:05:11
n (10^{10} cm^{-3})	8.2	1.0	2.2	2.3
L (10^3 km)	4.0	10.0	10.0	10.0
T (10^3 K)	7.0	10.0	9.5	12.0
$v_{\rm turb}$ (km/s)	6.5	9.0	16.2	20.0
$T_{\rm Ca}$ (10^3 K)	6.5	6.4	6.9	6.85
F(H$_\alpha$)	1.73(+6)	1.20(+6)	2.69(+6)	3.03(+6)
F(H$_\beta$)	5.49(+5)	1.57(+5)	5.94(+5)	5.89(+5)
H$_\alpha$/H$_\beta$	3.16	7.63	4.52	5.15
F(H)	6.55(+5)	3.02(+5)	6.18(+5)	8.08(+5)
F(H)/F(8542)	2.17	11.1	11.3	11.1
τ_α	1.49	0.26	0.89	0.71
$\tau_{\rm H}$	2.16	0.15	0.11	0.10

5 Conclusions

Within the framework of the heated gas model, the parameters of the matter of the studied prominence (Table 2) were obtained from the emission in three lines of hydrogen and the CaII ion for the time interval 7:52:46–08:05:11 UT. When analyzing the results, the following conclusions can be drawn:

1. The fluxes at all four time moments can be explained within the framework of the thermal model of homogeneous gas.
2. The increase in the steepness of the decrement (the ratio F(Hα)/F(Hβ)) is explained by a decrease in the optical

thickness in Hα, which is a consequence of an increase in the turbulent velocity $v_{\rm turb}$.
3. The gas temperature increases from 6–8 to 10–12 thousand K.
4. The column density of the gas does not change, which shows the small role of evaporation.
5. The temperature $T_{\rm Ca}$ increases, which indicates an increase in the flux of Lyman quanta.
6. Sufficiently large values of the flux ratios $F(\mathrm{H})/F(8542)$ and negligible calculated fluxes in HeI D3 do not contradict the observations during which the helium line and the calcium infrared line were not registered.

The authors thank the teams of the Solar Dynamics Observatory, GOES, and the Ondřejov Observatory for providing possibility to conduct observations and use the data.

References

Brown J.C., 1971. Solar Phys., vol. 18, p. 489.
Cunto W., Mendoza C., 1992. Rev. Mexicana Astron. Astrofis. vol. 23, p. 107.
Fletcher L. et al., 2011. Space Sci. Rev., vol. 159, p. 19.
Johnson L.C., 1972. Astrophys. J., vol. 174, p. 227.
Krucker S. et al., 2011. Astrophys. J., vol. 739, p. 96.
Melendez M., Bautista M.A., Badnell N.R., 2007. Astron. Astrophys., vol. 469, no. 3, p. 1203.
Seaton M.J., 1964. Planetary Space Sci., vol. 12, pp. 55–74.
Severnyi A.B., 1957. Soviet Astron., vol. 1, p. 668.
Xu Y., Cao W., Jing J., Wang H., 2012. Astrophys. J., vol. 750, p. L7.
Zimovets I.V., Kuznetsov S.A., Struminsky A.B., 2013. Astron. Lett., vol. 39, p. 267.